JOURNAL OF APPLIED ELECTROCHEMISTRY 12 (1982) 599–606

Solid state Li/MnO_2 cells

M. KANDA, S. YAMADA, T. SHIROGAMI, Y. SATO, T. TAKAMURA

Toshiba Research and Development Center, Toshiba Corporation, Saiwai-ku, Kawasaki 210, Japan

Received 11 November 1981

The possibility of using MnO_2 as the cathode material for a solid state lithium cell system has been studied. The cell system, where the mixture of MnO_2 and LiI is directly in contact with the lithium anode without a solid electrolyte layer, showed high cell voltage and low internal impedance. Cell behaviour for this system and the discharge mechanism were investigated and discussed. It may be considered that the discharge process consists of two reactions:

$$LiI + MnO_2 \rightarrow LiMn^{III}O_2 + (1/2)I_2$$

$$Li + (1/2)I_2 \rightarrow LiI.$$

The second reaction seems to determine the cell voltage.

1. Introduction

The recent remarkable progress in electronic devices has reduced the amount of current necessary to drive them. Accordingly, the requirement for commercial high energy density, high reliability, long life batteries is growing. To fulfil these needs, a number of solid state cell systems have been reported [1–3]. However, very few attempts have been made to use manganese dioxide as a cathode material for these systems [4], although it is well known to be an excellent cathode depolarizer, both for conventional batteries and the organic electrolyte Li/MnO_2 cell [5, 6].

This paper reports the possibility of using manganese dioxide as a cathode material for a solid state lithium cell system.

2. Experimental procedure

2.1. *Materials*

The manganese dioxide (MnO_2) powder used in this study was electrolytic manganese dioxide (EMD), classified to HMH (prepared for ordinary dry cells), and made by the Toyo Soda manufacturing company. The surface area of the powder was 67.9 $m^2 g^{-1}$, which was measured by the BET method (Perkin–Elmer, Model 212D). Average particle size was 25 μm and no particles larger than 100 μm were present (Leeds & Northrup, Microtrac).

In most cases, LiI was used as the solid electrolyte. Other solid electrolytes used were Li_3N, Li_2SO_4, $LiNbO_3$ and Li–β–alumina. These materials were either used as monophases or blended with each other.

A lithium foil of 0.5 mm thickness was used as the anode without special treatment of its surface. It was cut to size and put on the solid electrolyte or on the MnO_2 cathode directly.

2.2. *Heat treatment*

The MnO_2 was heat-treated in air at 230, 300, 350 or 450° C for eight hours to determine the best pretreatment conditions. The X-ray diffraction patterns for the heat-treated MnO_2 were obtained by using CuKα radiation.

The materials used for the solid electrolytes and other cell components were dried before constructing the cell. Solid LiI electrolyte was prepared from reagent grade LiI by heating at 100° C under vacuum for five hours.

2.3. *Cell construction*

The Li/MnO_2 cell used in this study was constructed as shown in Fig. 1. Cell construction and pellet preparation were similar to those reported

0021–891X/82/050599–07$03.34/0

in the literature [7]. The pelletizing pressure was 3500 kg cm^{-2} and the cell diameter was 13.0 mm. The cell was placed in a glass vessel filled with argon and all operations were carried out in an argon-filled dry box.

2.4. *Cell behaviour and electrolyte conductivity*

The Li/MnO_2 cell behaviour was investigated by discharging it with several constant resistance loads. The cell d.c. resistance was calculated from the current/voltage relationship at steady-state at low current (under 5 μA) discharge. Additionally, the cell a.c. impedance was obtained at 1 kHz frequency.

The electrolyte conductivity was measured both for d.c. and a.c. conditions. The conductivity cell used was one in which the electrolyte was sandwiched between two lithium metal foil electrodes. Otherwise the cell size and structure were the same as the Li/MnO_2 cell shown in Fig. 1. Constant direct current and alternating current at 1 kHz was supplied to the cell for the d.c. and a.c. electrolyte conductivity measurements, respectively.

3. Results and discussion

3.1. *Heat treatment effect*

Heat treatment of MnO_2, when used as a cathode material in an organic electrolyte Li/MnO_2 battery, is essential [5], because water adsorbed on to the MnO_2 surface and the crystal structure type may be important. This situation might also apply to solid state Li/MnO_2 cells.

The X-ray diffraction patterns observed for heat-treated MnO_2 at various temperatures were almost the same as those reported previously [5]; namely, γ-phase up to 230° C, a mixture of γ and β-phases at 300° C, and β-phase over 350° C. The weight loss by heat treatment was 2.7% at 250° C, 3.7% at 300° C and 4.5% at 350° C.

Figure 2 shows how the open circuit voltage (OCV) changes with time and the discharge curves with a 200 kΩ load at 25° C for the cell system Li/LiI/(MnO_2 + flake carbon [10%] + PTFE [5%]), where PTFE (polytetrafluoroethylene) is present as a binder. In each case, the initial OCV was over 2.7 V and the initial discharge voltage was over

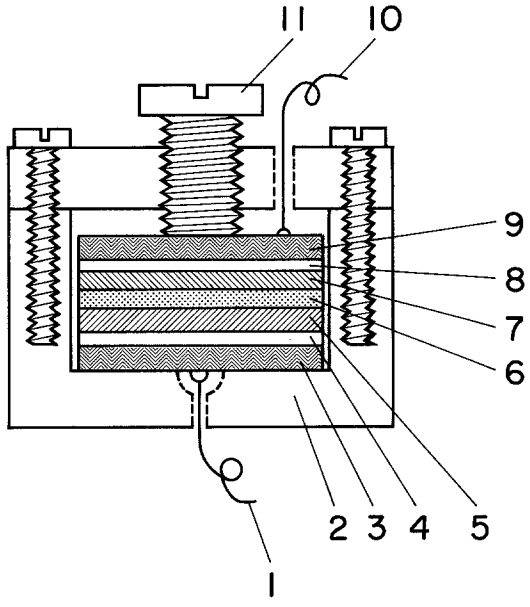

Fig. 1. Cell structure. 1, 10: Lead wire; 2: Lucite cover; 3, 9: Cu plate; 4, 8: Ni plate; 5: Cathode; 6: Solid electrolyte; 7: Li anode; 11: Bolt.

2 V. These facts indicate the possibility of using MnO_2 as a cathode material in a solid state cell system.

From Fig. 2, the best results were obtained using MnO_2 heat-treated at 230° C, for which the OCV was more stable and the voltage during discharge was the highest, well above 1 V. Accordingly, discussion will be limited to this 230° C heat-treated MnO_2.

3.2. *Compatibility of solid electrolytes with MnO_2*

Cell performances for solid state Li/MnO_2 systems with various electrolytes were investigated to evaluate their compatibility with MnO_2.

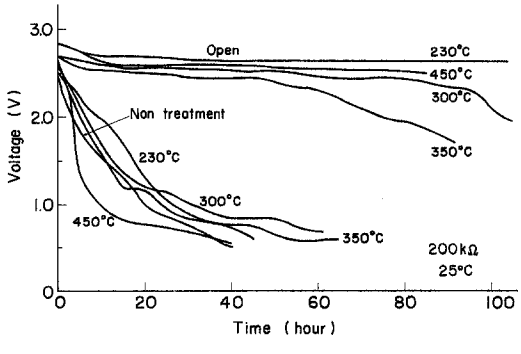

Fig. 2. MnO_2 heat treatment effect on Li/LiI/MnO_2 cells.

Table 1. Conductivity and cell performance for various solid electrolytes

Solid Electrolyte	*Condition*	*Thickness* (mm)	*Electrolyte resistivity*			*Cell* Li/S.E./MnO_2[c]	
			d.c. (kΩ)	*d.c.* ($\sigma \times 10^6$ S^{-1} cm^{-1})	*a.c.* (1 kHz) (kΩ)	OCV. (V)	dV/dI[d] (kΩ · cm^2)
LiI	Powder	0.55	44	0.93	41.5	2.87	50
LiI (80%) + RbI	Powder	1.43	650	0.17	217	2.93	580
LiI (66%) + α-Al_2O_3	Powder	0.80	756	0.08	720	2.92	1700
LiI (35%) + Li-β-alumina[a]	Powder	0.80	556	0.11	190	2.87	570
Li_2SO_4 (80.8%) + $LiNbO_3$[b]	Powder[a]	0.80	too large	–	–	2.65–3.40 (16 h)	12 000
Li_3N	Powder	0.50	24	2.2	30	1.52–1.97	280
Na-β-alumina	Sliced rod	0.45	non linear	–	–	2.90–2.32 (50 h)	–

[a] 75% of mobile Na is exchanged by Li.
[b] Li_2SO_4 and $LiNbO_3$ mixture was melted at 900° C and quenched, then milled.
[c] Cathode composition, MnO_2: Flake Carbon: PTFE = 85 : 10 : 5 in weight. Cell diameter is 13.0 mm. S.E. thicknesses are 0.7–0.8 mm
[d] $dV/dI = [V]/[A/cm^2] = \Omega \cdot cm^2$.

Table 1 shows the solid electrolytes tested and their properties. All the materials, except Na-β-alumina, are Li^+ conductors. Ohmic behaviour was observed during d.c. measurement with good reproducibility, except for Na-β-alumina. Li_3N showed the highest conductivity. Similar results were obtained by a.c. impedance measurement. Adding Al_2O_3 to LiI did not increase the LiI conductivity, despite reported results [8]. Conduction behaviour for Na-β-alumina was not ohmic under our measurement conditions and conductivity could not be defined. This might be explained as follows: Na-β-alumina was initially a Na^+ conductor, but slow replacement of Na^+ by Li^+ occurred during contact with the lithium electrode, gradually changing the shallow part of the electrolyte surface into an Li^+ conductor, and giving rise to time-dependent conductivity.

In Table 1, the cell behaviour for Li/MnO_2 with corresponding solid electrolytes is shown, for example, OCV values and internal impedance calculated from polarization curves at 25° C. In all cases, the thickness of the solid electrolytes was between 0.7 and 0.8 mm.

In the case of cells with an electrolyte containing LiI, the OCV was stable for a long time at 2.87–2.93 V. The cell $Li/(Li_2SO_4 + LiNbO_3)/MnO_2$ showed the highest OCV (3.5 V) 16 h after cell construction. This value is almost the same as that reported for the organic electrolyte Li/MnO_2 cell [9]. However, the cell showed too high an impedance due to the low conductivity of the electrolyte. The cell $Li/Li_3N/MnO_2$ showed rather a low voltage of 1.52 or 1.97 V, the OCV reproducibility of this system being poor. This fact suggests that MnO_2 decomposes Li_3N chemically to produce Li_2O [10], which blocks the Li^+ migration. The OCV of the cell Li/Na-β-alumina/MnO_2 changed slowly. After 50 h, 3.3 V was obtained. This also suggests the slow exchange of Na^+ with Li^+. From these results, it is concluded that of all the cell systems, only $Li/LiI/MnO_2$ has possible practical use.

3.3. *Reaction performance and reaction mechanism of Li/MnO_2 with LiI*

3.3.1. Performance of various systems. Based on the preceding results, modified Li/MnO_2 systems with LiI were investigated further.

Table 2 shows the systems considered, together with their OCV and internal impedance at 1 kHz. Roughly estimated thicknesses (in mm) for each layer are shown for each cell system. Conductivity of LiI [11, 12] used in these cells was between 0.9×10^{-6} and 1.2×10^{-6} S cm^{-1}. Cells A and B are basic cell systems, which have a pure LiI layer as the electrolyte. The OCV values for these sys-

Table 2. Various cell systems concerning LiI

System		OCV (V)	*Impedance at* 1 kHz (kΩ)
A	$\mathrm{Li}\left/\frac{\mathrm{LiI}}{0.5}\right/\frac{\mathrm{MnO_2 + fc + PTFE}\ \text{(a)}}{0.75}$	2.87–2.93	≃ 42.
B	$\mathrm{Li}\left/\frac{\mathrm{LiI}}{0.5}\right/\frac{\mathrm{MnO_2 + Pb}\ \text{(b)}}{0.75}$	2.96–2.88	≃ 41.
C	$\mathrm{Li}\left/\frac{\mathrm{LiI}}{0.6}\right/\frac{\mathrm{LiI + MnO_2}\ \text{(c)}}{0.75}$	2.70–2.85	≃ 71.
D	$\mathrm{Li}\left/\frac{\mathrm{LiI + MnO_2}}{0.75}\right/\frac{\mathrm{MnO_2 + fc + PTFE}\ \text{(a)}}{0.75}\ \text{(c)}$	3.05–2.90	≃ 28.
E	$\mathrm{Li}\left/\frac{\mathrm{LiI + MnO_2}\ \text{(c)}}{0.75}\right.$	2.40–2.50	≃ 10.
F	$\mathrm{Li}\left/\frac{\mathrm{MnO_2}}{0.80}\right.$	0.0083	≃ 78.

(a) MnO_2 : fc (Flake Carbon): PTFE = 85 : 10 : 5 in weight.
(b) MnO_2 : Pb = 80 : 20 in volume.
(c) LiI : MnO_2 = 2 : 1 in weight for (LiI + MnO_2) layer.
Numerical numbers indicate thicknesses (mm) of the layers underlined.

tems ranged from 2.87 to 2.96 V. The internal impedances were rather high, due to the high resistivity of the LiI electrolyte layer.

It is noteworthy that cell E, in which the cathode was a mixture of LiI and MnO_2, showed a rather high OCV of 2.4–2.5 V, although MnO_2 was directly in contact with the Li anode. Generally, direct contact between cathode and anode would bring about a decrease in the OCV. In fact, the OCV of cell F was almost zero. Therefore, it seems that some ion-conducting layer was formed on the surface of the lithium metal anode in cell E. The same consideration was applicable to cell D. Internal impedances of both cells E and D were much lower than those of cells A, B and C, because a LiI monophase layer was not involved in them.

Figure 3 shows voltage changes of the cells A, B, C, D and E for discharge with 1 MΩ load at 25° C. In the case of cell A, a sudden voltage drop from the plateau at 2.7 V to 2 V was observed within 70 h, and the voltage then decreased rapidly. Cell B behaved similarly. However, for cells C, D and E, no such voltage drops were observed. Since a layer consisting of a mixture of MnO_2 and LiI was present in those cells, the mixture was considered to work as an active cathode material. These results indicate that the MnO_2–LiI mixture would make a practical solid state Li/MnO_2 cell.

3.3.2. Lattice deformation of MnO_2. Figure 4 shows the X-ray diffraction patterns of cell components before and after discharge. Pattern 1 is for the (MnO_2 + fc + PTFE) layer of cells A and D before discharge. Patterns 2 and 3 are for the same layer of cells A and D after discharge. Pattern 4 is for the (LiI + MnO_2) layer of cell D after dis-

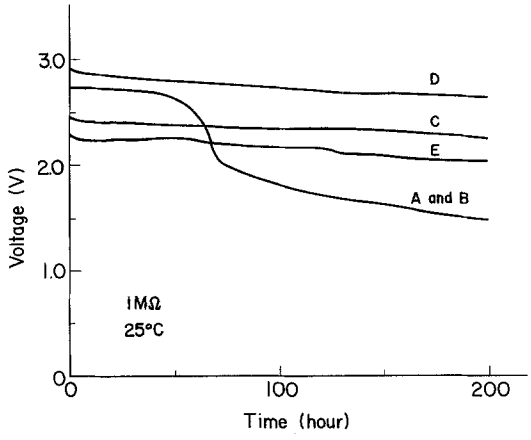

Fig. 3. Discharge curves for various systems.

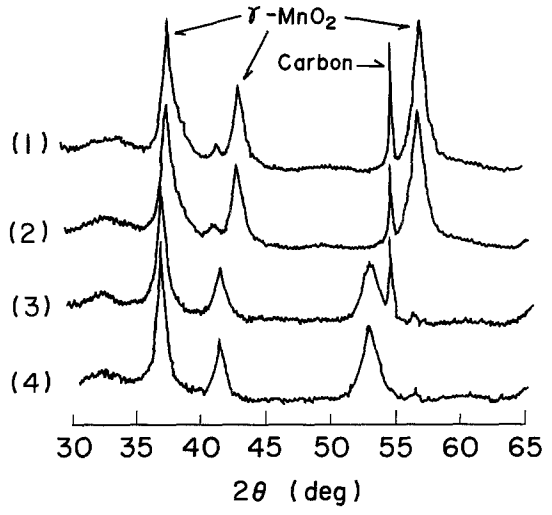

Fig. 4. MnO_2 X-ray diffraction patterns before and after discharge. 1. (MnO_2 + fc + PTFE) layer for cells A and D before discharge. 2. (MnO_2 + fc + PTFE) layer for cell A after discharge. 3. (MnO_2 + fc + PTFE) layer for cell D after discharge. 4. (LiI + MnO_2) layer for cell D after discharge.

charge. Discharged capacities for patterns 2 and 3 were 3.0 and 5.3% of the total MnO_2 capacity packed in the layers (MnO_2 + fc + PTFE), respectively, assuming the MnO_2 reduction valency to be 1.

Peaks in X-ray pattern 1 at $2\theta = 37.4°$, 42.9° and 56.9° corresponding to γ-phase MnO_2 for the layer (MnO_2 + fc + PTFE) were shifted to lower angles after discharge, as observed in patterns 2 and 3. The extent of peak shift between patterns 1 and 3 was larger than that between patterns 1 and 2. Peak shift for MnO_2 in the layer (LiI + MnO_2) was also observed, as shown in pattern 4. These results suggest that Li^+ was intercalated into the MnO_2 lattice during discharge [5], and the amount of Li^+ intercalated for cell D was larger than that for cell A.

The largest shift was found for the peak at 56.9° on the original pattern. As the γ-MnO_2 is a rutile (TiO_2) type crystal, this peak corresponds to the reflection from the ⟨2 2 1⟩ plane. Thus, it is considered that ⟨2 2 1⟩ lattice planes were expanded preferentially by Li^+ intercalation in the MnO_2 crystal.

3.3.3. Discharge mechanism. As shown above, the discharge product was the intercalation compound, in which Li^+ was inserted in to the MnO_2 lattice. X-ray diffraction results in our case were similar to those of the organic system [5], where the discharge product was speculated to be $(Mn^{III}O_2)(Li^+)$, not only from X-ray results but also from spectroscopic techniques. Thus, in the solid system the discharge product may likewise consist of $(Mn^{III}O_2)$ and (Li^+). It is possible to describe this compound as $LiMn^{III}O_2$ if in reduced MnO_2 $x = 1$ for Li_xMnO_2 [13, 14].

The formation process of $LiMn^{III}O_2$, however, may not be due to the electrochemical reaction proposed in the organic system as,

$$Li + MnO_2 + e \rightarrow LiMn^{III}O_2 \qquad (1)$$

because the OCV values for the solid systems were lower than the 3.3–3.5 V specified for Equation 1. The OCV results suggest [15] that the voltage determining reaction is

$$Li + (1/2)I_2 \rightarrow LiI, \qquad (2)$$

consisting of the two electrochemical reactions:

$$Li \rightarrow Li^+ + e \qquad (3)$$

and

$$(1/2)I_2 + e \rightarrow I^-. \qquad (4)$$

I_2 is produced by a reaction involving $LiMn^{III}O_2$,

$$LiI + MnO_2 \rightarrow LiMn^{III}O_2 + (1/2)I_2. \qquad (5)$$

Although thermodynamic data for such a solid phase reaction is lacking, this reaction appears reasonable from thermodynamic consideration of the following system of aqueous reactions [16]:

$$2MnO_2 + 2H^+ + 2e \rightleftharpoons Mn_2O_3 + H_2O$$

$$(E^0 = 1.014\,V \text{ versus NHE}) \qquad (6)$$

$$2I^- \rightleftharpoons I_2(c) + 2e$$

$$(E^0 = 0.536\,V \text{ versus NHE}). \qquad (7)$$

The standard potential of Equation 6 is more positive than that of Equation 7, so iodide ions (I^-) can be oxidized by MnO_2 to produce I_2. In fact, the dark brown colour of I_2 was observed on the walls of the glass vessel containing the MnO_2 and LiI mixture after a storage period of several days for a 33.3% MnO_2 mixture. This result likewise supports the possibility of Equation 5, and indicates that an I_2 vapour phase exists.

Assuming that Equations 2 and 5 are valid, the discharge reaction mechanism for the Li/(LiI + MnO_2) system, which corresponds to cell E in

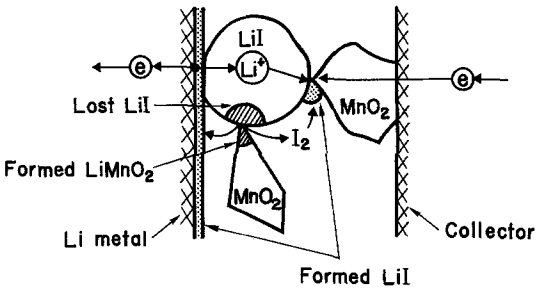

Fig. 5. Discharge reaction model for the Li/(LiI + MnO_2) system.

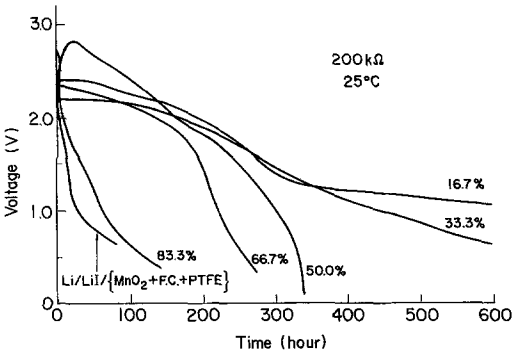

Fig. 6. Discharge curves for Li/LiI/(MnO_2 + fc + PTFE) and Li/(LiI + MnO_2) systems with various MnO_2 compositions (wt%).

Table 2, would be explained by the model shown in Fig. 5. I_2 vapour might be produced at an LiI/MnO_2 contact point, where MnO_2 reacts to form $LiMn^{III}O_2$ according to Equation 5. Initially, I_2 vapour would form a thin LiI film on the lithium metal anode, which would act as a solid electrolyte. This may explain why no short circuit was observed. Additionally, I_2 vapour might diffuse to other LiI/MnO_2 contact points, where I_2 would be electrochemically reduced to form a new LiI phase by accepting electrons from an MnO_2 particle and Li^+ from the original LiI phase. In this case, the MnO_2 particle would be serving as an electronic conductor (MnO_2 is a semiconductor, with a conductivity of about 8×10^{-2} Scm^{-1} [17]).

The above mechanism can be applied not only to cell E, but also to cells C and D, since these also involve a (LiI + MnO_2) layer. The mechanism is also applicable to cells A and B, since these cells also have LiI/MnO_2 contact interfaces, although their area is limited. The discharge process for cells A and B is considered to be as follows: I_2 is formed by Equation 5 at LiI/MnO_2 interfaces, but only in a limited volume, because of the limited interface area and the retarding effects of $LiMnO_2$ product build-up. When the cell is discharged, this I_2 is consumed via Equation 4, with the (MnO_2 + fc + PTFE) layer acting as a current collector. The I_2, however, is soon used up, with the reluctant sudden voltage drop seen in Fig. 3.

3.3.4. Discharge behaviour for the Li/(LiI + MnO_2) cell. Cell performance for Li/(LiI + MnO_2) systems was investigated on the basis of the foregoing discussions. Figure 6 and Table 3 show the discharge behaviours for Li/(LiI + MnO_2) systems with various MnO_2 contents at 25° C with a 200 kΩ load. Discharge times for cells in these systems were longer in all cases than that of the basic cell system Li/LiI/(MnO_2 + fc + PTFE). The working voltage remained above 2 V for over 200 h, with current densities of about 10 $\mu A\,cm^{-2}$, except for the cell with 83.3% MnO_2 content. Total discharge time increased as the MnO_2 content decreased. This indicates that MnO_2 utilization efficiency increases with increasing

Table 3. Li/(LiI + MnO_2) systems with various MnO_2 compositions

Composition (MnO_2 wt%)	OCV (V)	*Impedance at* 1 kHz (kΩ)	*Theoretical capacity*[a] (mAh)	*Discharge capacity*[b] (mAh)	*Utilization* (%)
16.7	2.64	~18	12.9	5.85	45.3
33.3	2.40	~6	25.7	4.93	19.2
50	1.97	~3	38.5	3.06	6.0
66.7	2.40	~2	51.4	2.33	4.5
83.3	2.56	~10	64.2	0.75	1.2

[a] Capacity calculated from MnO_2 content.
[b] 200 kΩ load. Discharge cut off voltage 0.5 V.

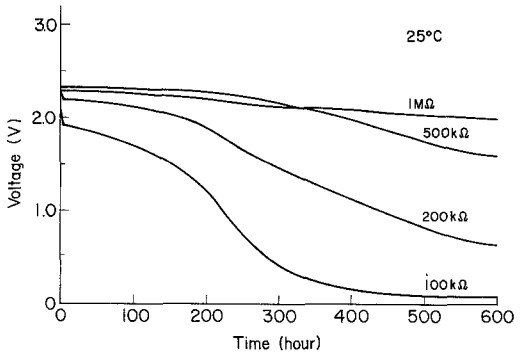

Fig. 7. Discharge curves for the Li/(LiI + MnO_2 [33.3 wt %]) system at various loads.

contact area of MnO_2 with LiI, which agrees with the above proposed mechanism.

Discharge curves for the cell system Li/(LiI + MnO_2) with 33.3% MnO_2 content are shown in Fig. 7. For a 1 MΩ load, the working voltage was maintained above 2 V for over 600 h. With a 100 kΩ load, the initial voltage was 1.8 V with a current density of about 15 $\mu A\,cm^{-2}$. Utilization efficiency in this case was 15.2%, and increased with increasing load resistance.

4. Conclusion

The possibilities of using MnO_2 as a cathode depolarizer were investigated for solid state lithium cell systems. It was shown that the mixture of LiI and MnO_2 could work as a cathode in a simple cell system Li/(LiI + MnO_2).

Acknowledgement

The authors wish to express their appreciation to Dr A. Imai for his helpful discussion.

References

[1] C. C. Liang and L. H. Barnette, *J. Electrochem. Soc.* **123** (1976) 453.
[2] A. A. Schneider, W. Greatbatch and R. Mead, *Power Sources* **5** (1970) 651.
[3] M. S. Whittingham, *J. Electrochem. Soc.* **123** (1976) 315.
[4] C. C. Liang and A. V. Joshi, U.S. application No. 790727 (1977) or Japanese Patent Kokai 53-133729.
[5] H. Ikeda, T. Saito and H. Tamura, 'Manganese Dioxide Symposium 1', Cleaveland, (1975) p. 384.
[6] *Idem, Denki Kagaku* **45** (1977) 314.
[7] C. R. Schlaikjer and C. C. Liang, *J. Electrochem. Soc.* **118** (1971) 1447.
[8] C. C. Liang, *ibid.* **120** (1973) 1289.
[9] T. Ohzuku, Z. Takehara and S. Yoshizawa, *Denki Kagaku* **46** (1978) 411.
[10] J. R. Rea and D. L. Foster, *Mater. Res. Bull* **14** (1979) 841.
[11] S. Pack, B. B. Owens and J. B. Wagner, Jr, Extended abstract of 155th meeting of the Electrochemical Society, (1979) p. 932.
[12] S. Lewkowitz, B. B. Owens and P. M. Skarstad, *ibid.* (1979) p. 23.
[13] D. W. Murphy, F. J. Di Salvo, J. N. Carides and J. V. Waszczak, *Mater. Res. Bull.* **13** (1978) 1395.
[14] M. Voinov, *J. Electrochem. Soc.* **128** (1981) 1822.
[15] B. Scrosati, *J. Appl. Electrochem.* **2** (1972) 231.
[16] M. Pourbaix, 'Atlas of Electrochemical Equilibrium in Aqueous Solutions', Pergamon Press, Oxford (1966).
[17] E. Preisler, *J. Appl. Electrochem.* **6** (1976) 311.